ROBOTICS:
Control, Sensing, Vision, and Intelligence

K. S. Fu
School of Electrical Engineering
Purdue University

R. C. Gonzalez
Department of Electrical Engineering
University of Tennessee
and
Perceptics Corporation
Knoxville, Tennessee

C. S. G. Lee
School of Electrical Engineering
Purdue University

McGraw-Hill Book Company
New York St. Louis San Francisco Auckland Bogotá
Hamburg Johannesburg London Madrid Mexico Milan Montreal New Delhi
Panama Paris São Paulo Singapore Sydney Tokyo Toronto

CHAPTER
SIX

SENSING

Art thou not sensible to feeling as to sight?
William Shakespeare

6.1 INTRODUCTION

The use of external sensing mechanisms allows a robot to interact with its environment in a flexible manner. This is in contrast to preprogrammed operation in which a robot is "taught" to perform repetitive tasks via a set of programmed functions. Although the latter is by far the most predominant form of operation of present industrial robots, the use of sensing technology to endow machines with a greater degree of intelligence in dealing with their environment is, indeed, an active topic of research and development in the robotics field. A robot that can "see" and "feel" is easier to train in the performance of complex tasks while, at the same time, requires less stringent control mechanisms than preprogrammed machines. A sensory, trainable system is also adaptable to a much larger variety of tasks, thus achieving a degree of universality that ultimately translates into lower production and maintenance costs.

The function of robot sensors may be divided into two principal categories: *internal state* and *external state*. Internal state sensors deal with the detection of variables such as arm joint position, which are used for robot control, as discussed in Chap. 5. External state sensors, on the other hand, deal with the detection of variables such as range, proximity, and touch. External sensing, the topic of Chaps. 6 to 8, is used for robot guidance, as well as for object identification and handling.

External state sensors may be further classified as *contact* or *noncontact* sensors. As their name implies, the former class of sensors respond to physical contact, such as touch, slip, and torque. Noncontact sensors rely on the response of a detector to variations in acoustic or electromagnetic radiation. The most prominent examples of noncontact sensors measure range, proximity, and visual properties of an object.

The focus of this chapter is on range, proximity, touch, and force-torque sensing. Vision sensors and techniques are discussed in detail in Chaps. 7 and 8. It is of interest to note that vision and range sensing generally provide gross guidance information for a manipulator, while proximity and touch are associated with the terminal stages of object grasping. Force and torque sensors are used as feedback devices to control manipulation of an object once it has been grasped (e.g., to avoid crushing the object or to prevent it from slipping).

6.2 RANGE SENSING

A range sensor measures the distance from a reference point (usually on the sensor itself) to objects in the field of operation of the sensor. Humans estimate distance by means of stereo visual processing, as discussed in Chap. 7, while other animals, such as bats, utilize the "time of flight" concept in which distance estimates are based on the time elapsed between the transmission and return of a sonic pulse. Range sensors are used for robot navigation and obstacle avoidance, where interest lies in estimating the distance to the closest objects, to more detailed applications in which the location and general shape characteristics of objects in the work space of a robot are desired. In this section we discuss several range sensing techniques that address these problems.

6.2.1 Triangulation

One of the simplest methods for measuring range is through triangulation techniques. This approach can be easily explained with the aid of Fig. 6.1. An object is illuminated by a narrow beam of light which is swept over the surface. The sweeping motion is in the plane defined by the line from the object to the detector and the line from the detector to the source. If the detector is focused on a *small* portion of the surface then, when the detector sees the light spot, its distance D to the illuminated portion of the surface can be calculated from the geometry of Fig. 6.1 since the angle of the source with the baseline and the distance B between the source and detector are known.

The above approach yields a point measurement. If the source-detector arrangement is moved in a fixed plane (up and down and sideways on a plane perpendicular to the paper and containing the baseline in Fig. 6.1), then it is possible

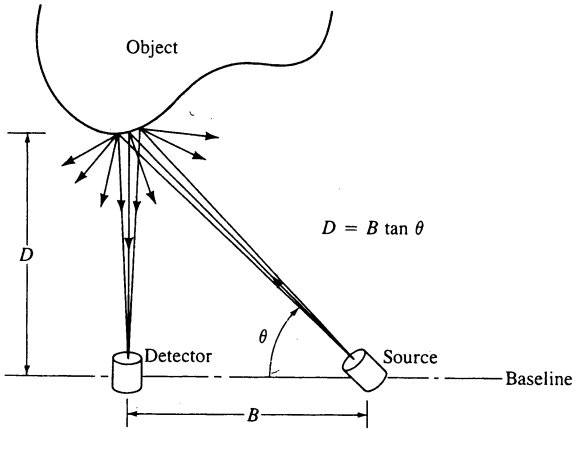

Figure 6.1 Range sensing by triangulation. (Adapted from Jarvis [1983*a*], © IEEE.)

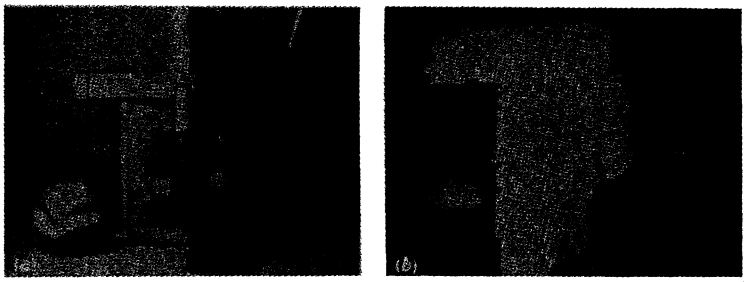

Figure 6.2 (*a*) An arrangement of objects scanned by a triangulation ranging device. (*b*) Corresponding image with intensities proportional to range. (From Jarvis [1983*a*], © IEEE.)

to obtain a set of points whose distances from the detector are known. These distances are easily transformed to three-dimensional coordinates by keeping track of the location and orientation of the detector as the objects are scanned. An example is shown in Fig. 6.2. Figure 6.2*a* shows an arrangement of objects scanned in the manner just explained. Figure 6.2*b* shows the results in terms of an image whose intensity (darker is closer) is proportional to the range measured from the plane of motion of the source-detector pair.

6.2.2 Structured Lighting Approach

This approach consists of projecting a light pattern onto a set of objects and using the distortion of the pattern to calculate the range. One of the most popular light patterns in use today is a sheet of light generated through a cylindrical lens or a narrow slit.

As illustrated in Fig. 6.3, the intersection of the sheet with objects in the work space yields a light stripe which is viewed through a television camera displaced a distance B from the light source. The stripe pattern is easily analyzed by a computer to obtain range information. For example, an inflection indicates a change of surface, and a break corresponds to a gap between surfaces.

Specific range values are computed by first calibrating the system. One of the simplest arrangements is shown in Fig. 6.3*b*, which represents a top view of Fig. 6.3*a*. In this arrangement, the light source and camera are placed at the same height, and the sheet of light is perpendicular to the line joining the origin of the light sheet and the center of the camera lens. We call the vertical plane containing this line the *reference plane.* Clearly, the reference plane is perpendicular to the sheet of light, and any vertical flat surface that intersects the sheet will produce a vertical stripe of light (see Fig. 6.3*a*) in which every point will have the same perpendicular distance to the reference plane. The objective of the arrangement shown in Fig. 6.3*b* is to position the camera so that every such vertical stripe also appears vertical in the image plane. In this way, every point along the same column in the image will be known to have the same distance to the reference plane.

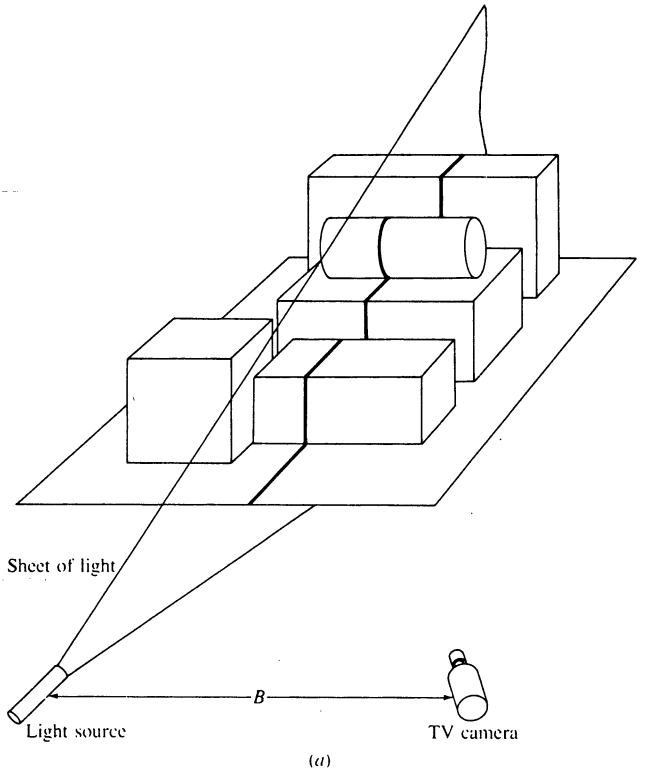

Figure 6.3 (*a*) Range measurement by structured lighting approach. (*b*) Top view of part (*a*) showing a specific arrangement which simplifies calibration.

Most systems based on the sheet-of-light approach use digital images. Suppose that the image seen by the camera is digitized into an $N \times M$ array (see Sec. 7.2), and let $y = 0, 1, 2, \ldots, M - 1$ be the column index of this array. As explained below, the calibration procedure consists of measuring the distance B between the light source and lens center, and then determining the angles α_c and α_0. Once these quantities are known, it follows from elementary geometry that d in Fig. 6.3*b* is given by

$$d = \lambda \tan \theta \tag{6.2-1}$$

where λ is the focal length of the lens and

$$\theta = \alpha_c - \alpha_0 \tag{6.2.2}$$

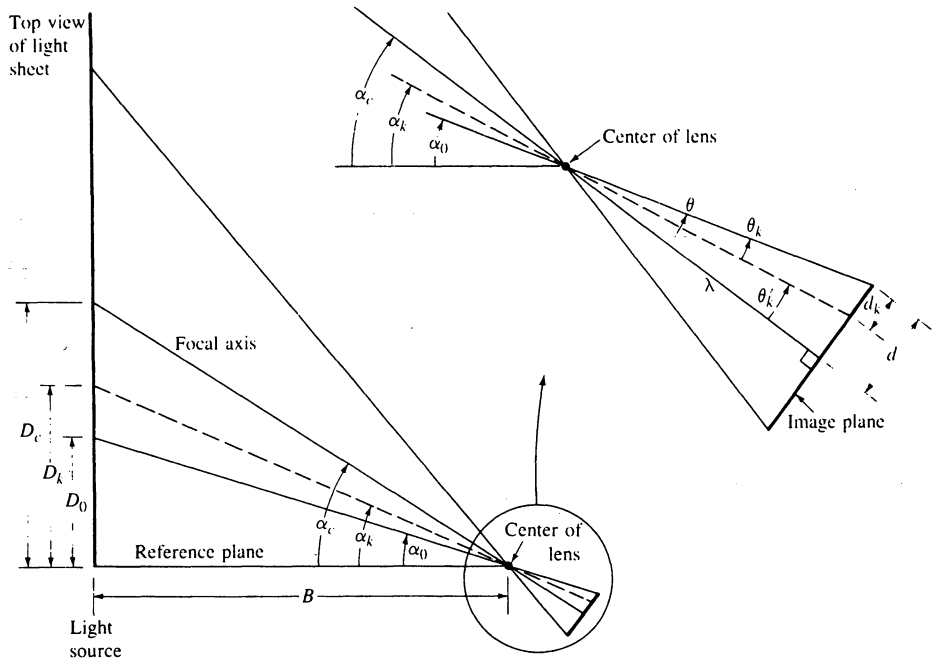

(*b*)

Figure 6.3 (continued)

For an M-column digital image, the distance increment d_k between columns is given by

$$d_k = k\,\frac{d}{M/2} = \frac{2kd}{M} \tag{6.2-3}$$

for $0 \leqslant k \leqslant M/2$. (In an image viewed on a monitor, $k = 0$ would correspond to the leftmost column and $k = M/2$ to the center column.) The angle α_k made by the projection of an arbitrary stripe is easily obtained by noting that

$$\alpha_k = \alpha_c - \theta_k' \tag{6.2-4}$$

where

$$\tan\theta_k' = \frac{d - d_k}{\lambda} \tag{6.2-5}$$

or, using Eq. (6.2-3),

$$\theta_k' = \tan^{-1}\left[\frac{d(M - 2k)}{M\lambda}\right] \tag{6.2-6}$$

where $0 \leqslant k \leqslant M/2$. For the remaining values of k (i.e., on the other side of the optical axis), we have

$$\alpha_k = \alpha_c + \theta_k'' \tag{6.2-7}$$

where

$$\theta_k'' = \tan^{-1}\left[\frac{d(2k - M)}{M\lambda}\right] \tag{6.2-8}$$

for $M/2 < k \leqslant (M - 1)$.

By comparing Eqs. (6.2-6) and (6.2-8) we note that $\theta_k'' = -\theta_k'$, so Eqs. (6.2-4) and (6.2-7) are identical for the *entire* range $0 \leqslant k \leqslant M - 1$. It then follows from Fig. 6.3*b* that the perpendicular distance D_k between an arbitrary light stripe and the reference plane is given by

$$D_k = B \tan \theta_k \tag{6.2-9}$$

for $0 \leqslant k \leqslant M - 1$, where α_k is given either by Eq. (6.2-4) or (6.2-7).

It is important to note that once B, α_0, α_c, M, and λ are known, the column number in the digital image completely determines the distance between the reference plane and all points in the stripe imaged on that column. Since M and λ are fixed parameters, the calibration procedure consists simply of measuring B and determining α_c and α_0, as indicated above. To determine α_c, we place a flat vertical surface so that its intersection with the sheet of light is imaged on the center of the image plane (i.e., at $y = M/2$). We then physically measure the perpendicular distance D_c between the surface and the reference plane. From the geometry of Fig. 6.3*b* it follows that

$$\alpha_c = \tan^{-1}\left[\frac{D_c}{B}\right] \tag{6.2-10}$$

In order to determine α_0, we move the surface closer to the reference plane until its light stripe is imaged at $y = 0$ on the image plane. We then measure D_0 and, from Fig. 6.3*b*,

$$\alpha_0 = \tan^{-1}\left[\frac{D_0}{B}\right] \tag{6.2-11}$$

This completes the calibration procedure.

The principal advantage of the arrangement just discussed is that it results in a relatively simple range measuring technique. Once calibration is completed, the distance associated with every column in the image is computed using Eq. (6.2-9) with $k = 0, 1, 2, \ldots, M - 1$ and the results are stored in memory. Then, during normal operation, the distance of any imaged point is obtained simply by deter-

mining its column number in the image and addressing the corresponding location in memory.

Before leaving this section, we point out that it is possible to use the concepts discussed in Sec. 7.4 to solve a more general problem in which the light source and camera are placed arbitrarily with respect to each other. The resulting expressions, however, would be considerably more complicated and difficult to handle from a computational point of view.

6.2.3 Time-of-Flight Range Finders

In this section we discuss three methods for determining range based on the time-of-flight concept introduced at the beginning of Sec. 6.2. Two of the methods utilize a laser, while the third is based on ultrasonics.

One approach for using a laser to determine range is to measure the time it takes an emitted pulse of light to return coaxially (i.e., along the same path) from a reflecting surface. The distance to the surface is given by the simple relationship $D = cT/2$, where T is the pulse transit time and c is the speed of light. It is of interest to note that, since light travels at approximately 1 ft/ns, the supporting electronic instrumentation must be capable of 50-ps time resolution in order to achieve a $\pm$ ¼-inch accuracy in range.

A pulsed-laser system described by Jarvis [1983*a*] produces a two-dimensional array with values proportional to distance. The two-dimensional scan is accomplished by deflecting the laser light via a rotating mirror. The working range of this device is on the order of 1 to 4 m, with an accuracy of $\pm$ 0.25 cm. An example of the output of this system is shown in Fig. 6.4. Part (*a*) of this figure shows a collection of three-dimensional objects, and Fig. 6.4*b* is the corresponding sensed array displayed as an image in which the intensity at each point is proportional to the distance between the sensor and the reflecting surface at that point (darker is closer). The bright areas around the object boundaries represent discontinuity in range determined by postprocessing in a computer.

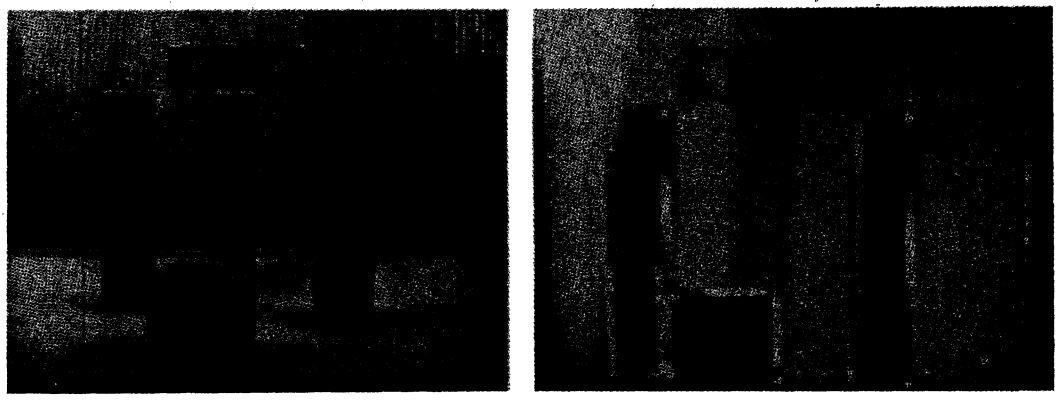

Figure 6.4 (*a*) An arrangement of objects. (*b*) Image with intensity proportional to range. (From Jarvis [1983*b*], © IEEE.)

An alternative to pulsed light is to use a continuous-beam laser and measure the delay (i.e., phase shift) between the outgoing and returning beams. We illustrate this concept with the aid of Fig. 6.5. Suppose that a beam of laser light of wavelength λ is split into two beams. One of these (called the *reference beam*) travels a distance L to a phase measuring device, and the other travels a distance D out to a reflecting surface. The total distance traveled by the reflected beam is $D' = L + 2D$. Suppose that $D = 0$. Under this condition $D' = L$ and both the reference and reflected beams arrive simultaneously at the phase measuring device. If we let D increase, the reflected beam travels a longer path and, therefore, a phase shift is introduced between the two beams at the point of measurement, as illustrated in Fig. 6.5*b*. In this case we have that

$$D' = L + \frac{\theta}{360}\lambda \tag{6.2-12}$$

It is noted that if $\theta = 360°$ the two waveforms are again aligned and we cannot differentiate between $D' = L$ and $D' = L + n\lambda$, $n = 1, 2, \ldots$, based on measurements of phase shift alone. Thus, a unique solution can be obtained only if we

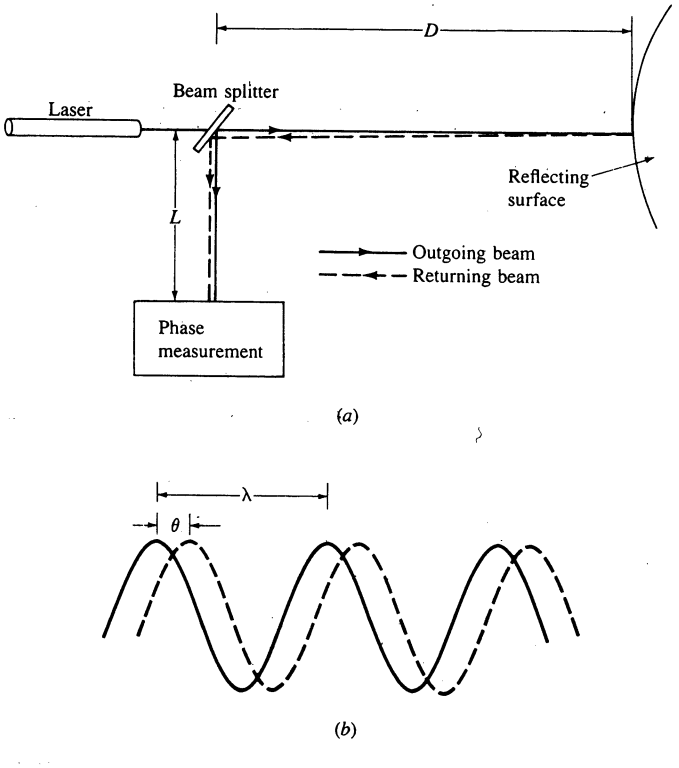

Figure 6.5 (*a*) Principles of range measurement by phase shift. (*b*) Shift between outgoing and returning light waveforms.

require that $\theta < 360°$ or, equivalently, that $2D < \lambda$. Since $D' = L + 2D$, we have by substitution into Eq. (6.2-12) that

$$D = \frac{\theta}{360}\left[\frac{\lambda}{2}\right] \tag{6.2-13}$$

which gives distance in terms of phase shift if the wavelength is known.

Since the wavelength of laser light is small (e.g., 632.8 nm for a helium-neon laser), the method sketched in Fig. 6.5 is impractical for robotic applications. A simple solution to this problem is to modulate the amplitude of the laser light by using a waveform of much higher wavelength. (For example, recalling that $c = f\lambda$, a modulating sine wave of frequency $f = 10\,\text{MHz}$ has a wavelength of 30m.) The approach is illustrated in Fig. 6.6. The basic technique is as before, but the reference signal is now the modulating function. The modulated laser signal is sent out to the target and the returning beam is stripped of the modulating signal, which is then compared against the reference to determine phase shift. Equation (6.2-13) still holds, but we are now working in a more practical range of wavelengths.

An important advantage of the continuous vs. the pulsed-light technique is that the former yields intensity as well as range information (Jarvis [1983*a*]). However, continuous systems require considerably higher power. Uncertainties in distance measurements obtained by either technique require averaging the returned signal to reduce the error. If we treat the problem as that of measurement noise being added to a true distance, and we assume that measurements are statistically independent, then it can be shown that the standard deviation of the average is equal to $1/\sqrt{N}$ times the standard deviation of the noise, where N is the number of samples averaged. In other words, the longer we average, the smaller the uncertainty will be in the distance estimate.

An example of results obtainable with a continuous, modulated laser beam scanned by a rotating mirror is shown in Fig. 6.7*b*. Part (*a*) of this figure is the range array displayed as an intensity image (brighter is closer). The true intensity information obtained with the same device is shown in part (*b*). Note that these two images complement each other. For example, it is difficult to count the

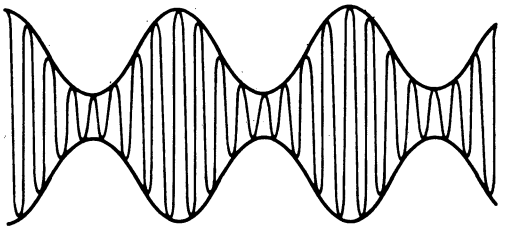

Figure 6.6 Amplitude-modulated waveform. Note the much larger wavelength of the modulating function.

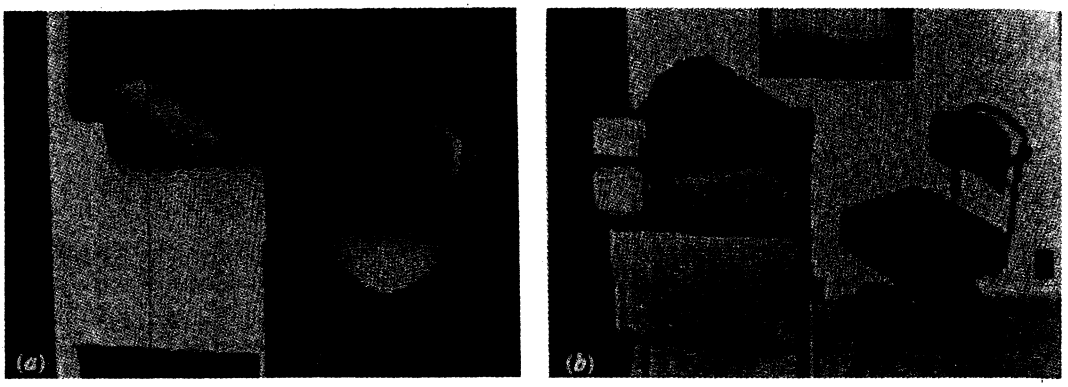

Figure 6.7 (*a*) Range array displayed as an image. (*b*) Intensity image. (From Duda, Nitzan, and Barrett [1979], © IEEE.)

number of objects on top of the desk in Fig. 6.7*a*, a simple task in the intensity image. Conversely, it is not possible to determine the distance between the near and far edges of the desk top by examining the intensity image, while this information is readily available in the range array. Techniques for processing this type of information are discussed in Chaps. 7 and 8.

An ultrasonic range finder is another major exponent of the time-of-flight concept. The basic idea is the same as that used with a pulsed laser. An ultrasonic chirp is transmitted over a short time period and, since the speed of sound is known for a specified medium, a simple calculation involving the time interval between the outgoing pulse and the return echo yields an estimate of the distance to the reflecting surface.

In an ultrasonic ranging system manufactured by Polaroid, for example, a 1-ms chirp, consisting of 56 pulses at four frequencies, 50, 53, 57, and 60 KHz, is transmitted by a transducer 1½ inches in diameter. The signal reflected by an object is detected by the same transducer and processed by an amplifier and other circuitry capable of measuring range from approximately 0.9 to 35 ft, with an accuracy of about 1 inch. The mixed frequencies in the chirp are used to reduce signal cancellation. The beam pattern of this device is around 30°, which introduces severe limitations in resolution if one wishes to use this device to obtain a range image similar to those discussed earlier in this section. This is a common problem with ultrasonic sensors and, for this reason, they are used primarily for navigation and obstacle avoidance. The construction and operational characteristics of ultrasonic sensors are discussed in further detail in Sec. 6.3.

6.3 PROXIMITY SENSING

The range sensors discussed in the previous section yield an estimate of the distance between a sensor and a reflecting object. Proximity sensors, on the other hand, generally have a binary output which indicates the presence of an object

within a specified distance interval. Typically, proximity sensors are used in robotics for near-field work in connection with object grasping or avoidance. In this section we consider several fundamental approaches to proximity sensing and discuss the basic operational characteristics of these sensors.

6.3.1 Inductive Sensors

Sensors based on a change of inductance due to the presence of a metallic object are among the most widely used industrial proximity sensors. The principle of operation of these sensors can be explained with the aid of Figs. 6.8 and 6.9. Figure 6.8*a* shows a schematic diagram of an inductive sensor which basically consists of a wound coil located next to a permanent magnet packaged in a simple, rugged housing.

The effect of bringing the sensor in close proximity to a ferromagnetic material causes a change in the position of the flux lines of the permanent magnet, as shown in Fig. 6.8*b* and *c*. Under static conditions there is no movement of the flux lines and, therefore, no current is induced in the coil. However, as a ferromagnetic object enters or leaves the field of the magnet, the resulting change in

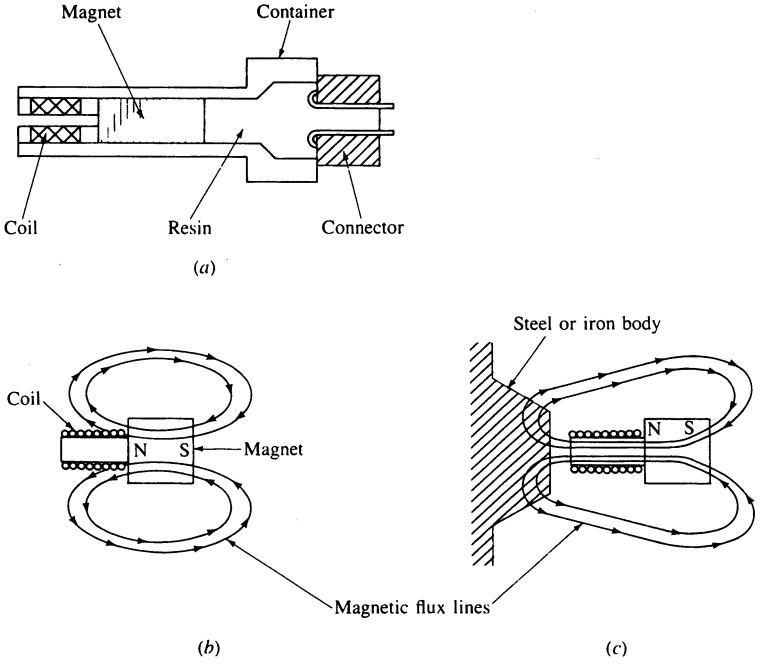

Figure 6.8 (*a*) An inductive sensor. (*b*) Shape of flux lines in the absence of a ferromagnetic body. (*c*) Shape of flux lines when a ferromagnetic body is brought close to the sensor. (Adapted from Canali [1981*a*], © Società Italiana di Fisica.)

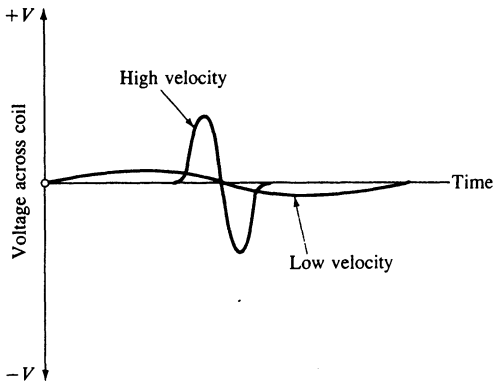

(*a*)

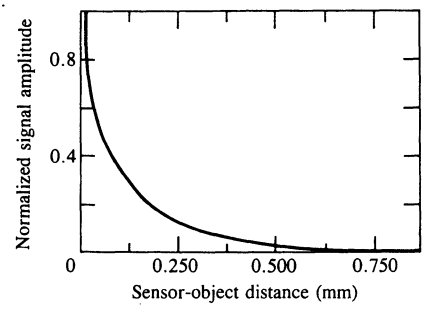

(*b*)

Figure 6.9 (*a*) Inductive sensor response as a function of speed. (*b*) Sensor response as a function of distance. (Adapted from Canali [1981*a*], © Società Italiana di Fisica.)

the flux lines induces a current pulse whose amplitude and shape are proportional to the rate of change in the flux.

The voltage waveform observed at the output of the coil provides an effective means for proximity sensing. Figure 6.9*a* illustrates how the voltage measured across the coil varies as a function of the speed at which a ferromagnetic material is introduced in the field of the magnet. The polarity of the voltage out of the sensor depends on whether the object is entering or leaving the field. Figure 6.9*b* illustrates the relationship between voltage amplitude and sensor-object distance. It is noted from this figure that sensitivity falls off rapidly with increasing distance, and that the sensor is effective only for fractions of a millimeter.

Since the sensor requires motion to produce an output waveform, one approach for generating a binary signal is to integrate this waveform. The binary output remains low as long as the integral value remains below a specified threshold, and then switches to high (indicating proximity of an object) when the threshold is exceeded.

6.3.2 Hall-Effect Sensors

The reader will recall from elementary physics that the Hall effect relates the voltage between two points in a conducting or semiconducting material to a magnetic field across the material. When used by themselves, Hall-effect sensors can only detect magnetized objects. However, when used in conjunction with a permanent magnet in a configuration such as the one shown in Fig. 6.10, they are capable of detecting all ferromagnetic materials. When used in this way, a Hall-effect device senses a strong magnetic field in the absence of a ferromagnetic metal in the near field (Fig. 6.10*a*). When such a material is brought in close proximity with the device, the magnetic field weakens at the sensor due to bending of the field lines through the material, as shown in Fig. 6.10*b*.

Hall-effect sensors are based on the principle of a Lorentz force which acts on a charged particle traveling through a magnetic field. This force acts on an axis perpendicular to the plane established by the direction of motion of the charged particle and the direction of the field. That is, the Lorentz force is given by $\mathbf{F} = q(\mathbf{v} \times \mathbf{B})$ where q is the charge, $\mathbf{v}$ is the velocity vector, $\mathbf{B}$ is the magnetic field vector, and "$\times$" is the vector cross product. Suppose, for example, that a current flows through a doped, n-type semiconductor which is immersed in a magnetic field, as shown in Fig. 6.11. Recalling that electrons are the majority carriers in n-type materials, and that conventional current flows opposite to electron current, we would have that the force acting on the moving, negatively charged particles would have the direction shown in Fig. 6.11. This force would act on the electrons, which would tend to collect at the bottom of the material and thus produce a voltage across it which, in this case, would be positive at the top.

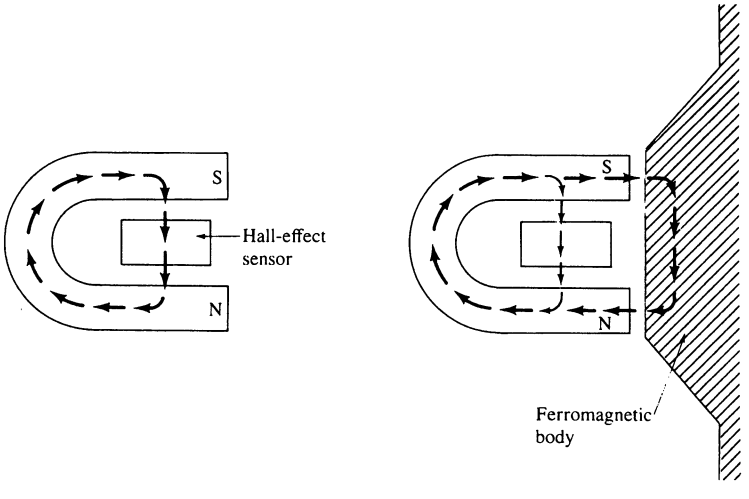

Figure 6.10 Operation of a Hall-effect sensor in conjunction with a permanent magnet. (Adapted from Canali [1981*a*], © Società Italiana di Fisica.)

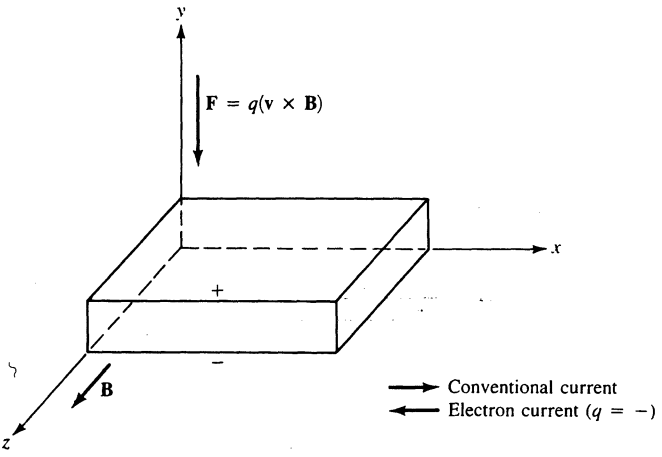

Figure 6.11 Generation of Hall voltage.

Bringing a ferromagnetic material close to the semiconductor-magnet device would decrease the strength of the magnetic field, thus reducing the Lorentz force and, ultimately, the voltage across the semiconductor. This drop in voltage is the key for sensing proximity with Hall-effect sensors. Binary decisions regarding the presence of an object are made by thresholding the voltage out of the sensor.

It is of interest to note that using a semiconductor, such as silicon, has a number of advantages in terms of size, ruggedness, and immunity to electrical interference. In addition, the use of semiconducting materials allows the construction of electronic circuitry for amplification and detection directly on the sensor itself, thus reducing sensor size and cost.

6.3.3 Capacitive Sensors

Unlike inductive and Hall-effect sensors which detect only ferromagnetic materials, capacitive sensors are potentially capable (with various degrees of sensitivity) of detecting all solid and liquid materials. As their name implies, these sensors are based on detecting a change in capacitance induced by a surface that is brought near the sensing element.

The basic components of a capacitive sensor are shown in Fig. 6.12. The sensing element is a capacitor composed of a sensitive electrode and a reference electrode. These can be, for example, a metallic disk and ring separated by a dielectric material. A cavity of dry air is usually placed behind the capacitive element to provide isolation. The rest of the sensor consists of electronic circuitry which can be included as an integral part of the unit, in which case it is normally embedded in a resin to provide sealing and mechanical support.

There are a number of electronic approaches for detecting proximity based on a change in capacitance. One of the simplest includes the capacitor as part of an

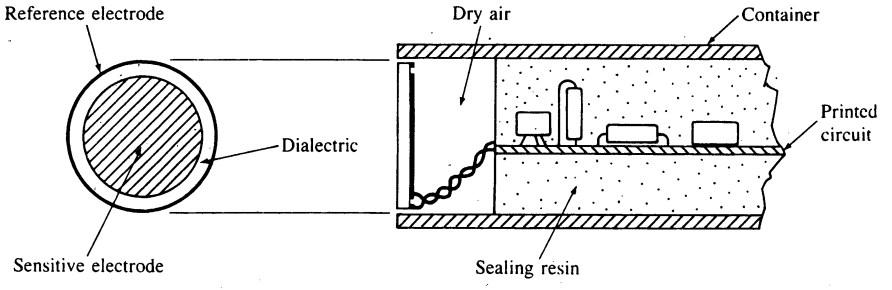

Figure 6.12 A capacitive proximity sensor. (From Canali [1981*a*], © Società Italiana di Fisica.)

oscillator circuit designed so that the oscillation starts only when the capacitance of the sensor exceeds a predefined threshold value. The start of oscillation is then translated into an output voltage which indicates the presence of an object. This method provides a binary output whose triggering sensitivity depends on the threshold value.

A more complicated approach utilizes the capacitive element as part of a circuit which is continuously driven by a reference sinusoidal waveform. A change in capacitance produces a phase shift between the reference signal and a signal derived from the capacitive element. The phase shift is proportional to the change in capacitance and can thus be used as a basic mechanism for proximity detection.

Figure 6.13 illustrates how capacitance varies as a function of distance for a proximity sensor based on the concepts just discussed. It is of interest to note that sensitivity decreases sharply past a few millimeters, and that the shape of the response curve depends on the material being sensed. Typically, these sensors are

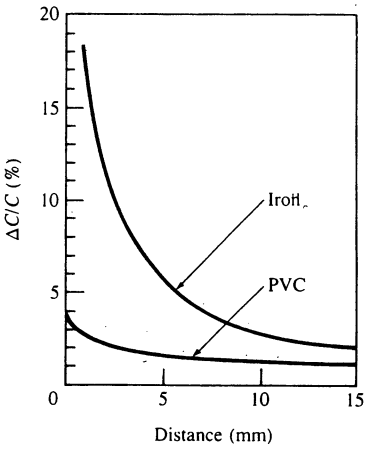

Figure 6.13 Response (percent change in capacitance) of a capacitive proximity sensor as a function of distance. (From Canali [1981*a*], © Società Italiana di Fisica.)

operated in a binary mode so that a change in the capacitance greater than a preset threshold T indicates the presence of an object, while changes below the threshold indicate the absence of an object with respect to detection limits established by the value of T.

6.3.4 Ultrasonic Sensors

The response of all the proximity sensors discussed thus far depends strongly on the material being sensed. This dependence can be reduced considerably by using ultrasonic sensors, whose operation for range detection was introduced briefly at the end of Sec. 6.2.3. In this section we discuss in more detail the construction and operation of these sensors and illustrate their use for proximity sensing.

Figure 6.14 shows the structure of a typical ultrasonic transducer used for proximity sensing. The basic element is an electroacoustic transducer, often of the piezoelectric ceramic type. The resin layer protects the transducer against humidity, dust, and other environmental factors; it also acts as an acoustical impedance matcher. Since the same transducer is generally used for both transmitting and receiving, fast damping of the acoustic energy is necessary to detect objects at close range. This is accomplished by providing acoustic absorbers, and by decoupling the transducer from its housing. The housing is designed so that it produces a narrow acoustic beam for efficient energy transfer and signal directionality.

The operation of an ultrasonic proximity sensor is best understood by analyzing the waveforms used for both transmission and detection of the acoustic energy signals. A typical set of waveforms is shown in Fig. 6.15. Waveform A is the gating signal used to control transmission. Waveform B shows the output signal as well as the resulting echo signal. The pulses shown in C result either upon transmission or reception. In order to differentiate between pulses corresponding to outgoing and returning energy, we introduce a time window (waveform D) which in essence establishes the detection capability of the sensor. That is, time interval Δt_1 is the minimum detection time, and $\Delta t_1 + \Delta t_2$ the maximum. (It is noted that these time intervals are equivalent to specifying distances since the pro-

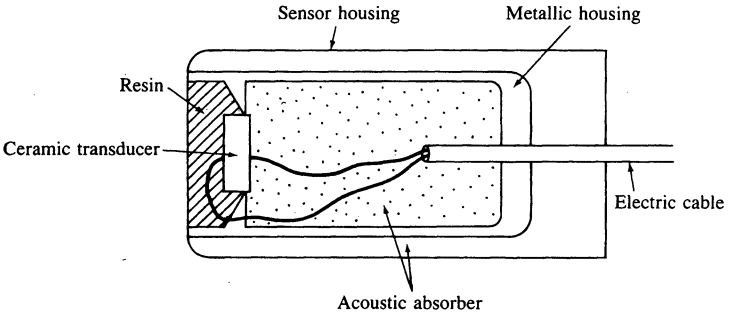

Figure 6.14 An ultrasonic proximity sensor. (Adapted from Canali [1981*b*], © Elsevier Sequoia.)

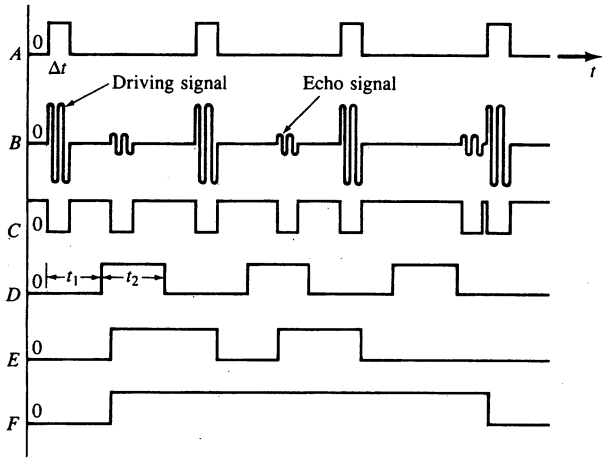

Figure 6.15 Waveforms associated with an ultrasonic proximity sensor. (Adapted from Canali [1981*b*], © Elsevier Sequoia.)

pagation velocity of an acoustic wave is known given the transmission medium.) An echo received while signal *D* is high produces the signal shown in *E*, which is reset to low at the end of a transmission pulse in signal *A*. Finally, signal *F* is set high on the positive edge of a pulse in *E* and is reset to low when *E* is low *and* a pulse occurs in *A*. In this manner, *F* will be high whenever an object is present in the distance interval specified by the parameters of waveform *D*. That is, *F* is the output of interest in an ultrasonic sensor operating in a binary mode.

6.3.5 Optical Proximity Sensors

Optical proximity sensors are similar to ultrasonic sensors in the sense that they detect proximity of an object by its influence on a propagating wave as it travels from a transmitter to a receiver. One of the most common approaches for detecting proximity by optical means is shown in Fig. 6.16. This sensor consists of a solid-state light-emitting diode (LED), which acts as a transmitter of infrared light, and a solid-state photodiode which acts as the receiver. The cones of light formed by focusing the source and detector on the same plane intersect in a long, pencil-like volume. This volume defines the field of operation of the sensor since a reflective surface which intersects the volume is illuminated by the source and simultaneously "seen" by the receiver.

Although this approach is similar in principle to the triangulation method discussed in Sec. 6.2.1, it is important to note that the detection volume shown in Fig. 6.16 does not yield a point measurement. In other words, a surface located *anywhere* in the volume will produce a reading. While it is possible to calibrate the intensity of these readings as a function of distance for known object orientations and reflective characteristics, the typical application of the arrangement

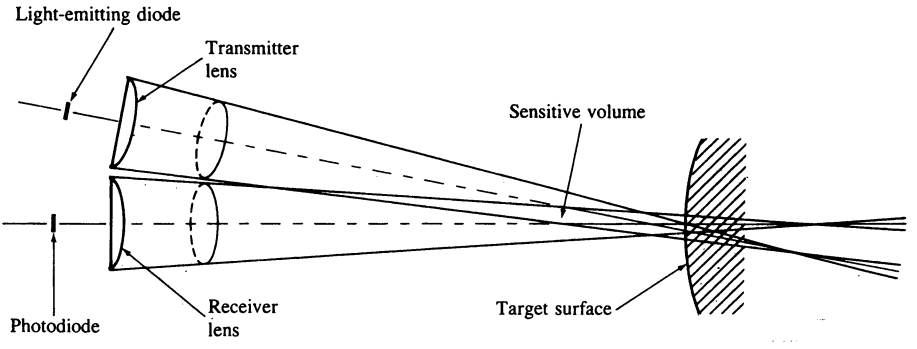

Figure 6.16 Optical proximity sensor. (From Rosen and Nitzan [1977], © IEEE.)

shown in Fig. 6.16 is in a mode where a binary signal is generated when the received light intensity exceeds a threshold value.

6.4 TOUCH SENSORS

Touch sensors are used in robotics to obtain information associated with the contact between a manipulator hand and objects in the workspace. Touch information can be used, for example, for object location and recognition, as well as to control the force exerted by a manipulator on a given object. Touch sensors can be subdivided into two principal categories: binary and analog. Binary sensors are basically switches which respond to the presence or absence of an object. Analog sensors, on the other hand, output a signal proportional to a local force. These devices are discussed in more detail in the following sections.

6.4.1 Binary Sensors

As indicated above, binary touch sensors are contact devices, such as microswitches. In the simplest arrangement, a switch is placed on the inner surface of each finger of a manipulator hand, as illustrated in Fig. 6.17. This type of sensing is useful for determining if a part is present between the fingers. By moving the hand over an object and sequentially making contact with its surface, it is also possible to center the hand over the object for grasping and manipulation.

Multiple binary touch sensors can be used on the inside surface of each finger to provide further tactile information. In addition, they are often mounted on the external surfaces of a manipulator hand to provide control signals useful for guiding the hand throughout the work space. This latter use of touch sensing is analogous to what humans do in feeling their way in a totally dark room.

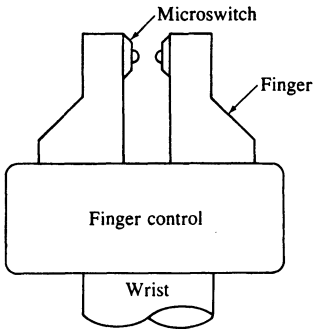

Figure 6.17 A simple robot hand equipped with binary touch sensors.

6.4.2 Analog Sensors

An analog touch sensor is a compliant device whose output is proportional to a local force. The simplest of these devices consists of a spring-loaded rod (Fig. 6.18) which is mechanically linked to a rotating shaft in such a way that the displacement of the rod due to a lateral force results in a proportional rotation of the shaft. The rotation is then measured continuously using a potentiometer or digitally using a code wheel. Knowledge of the spring constant yields the force corresponding to a given displacement.

During the past few years, considerable effort has been devoted to the development of tactile sensing arrays capable of yielding touch information over a wider area than that afforded by a single sensor. The use of these devices is illustrated in Fig. 6.19, which shows a robot hand in which the inner surface of each

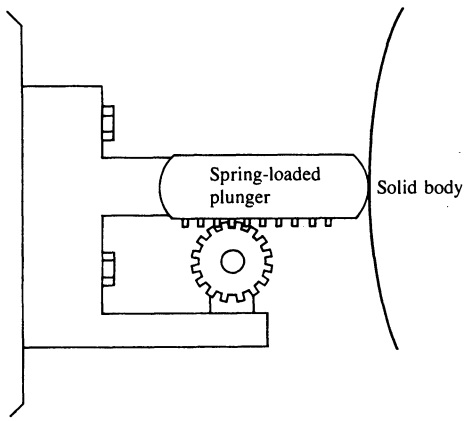

Figure 6.18 A basic analog touch sensor.

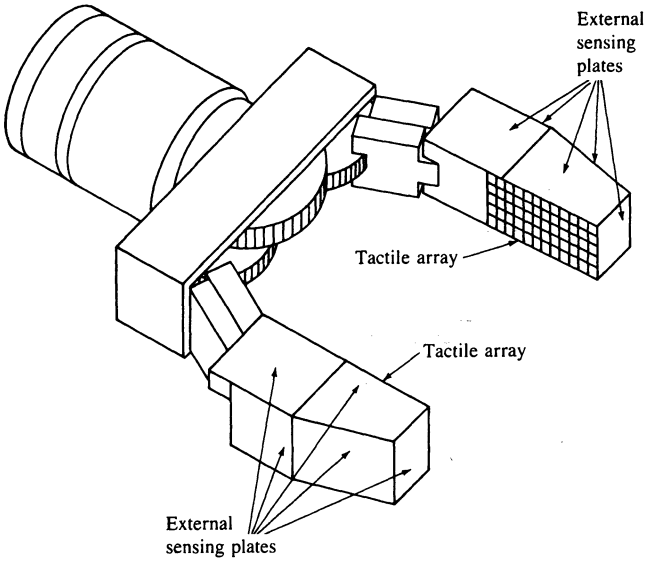

Figure 6.19 A robot hand equipped with tactile sensing arrays.

finger has been covered with a tactile sensing array. The external sensing plates are typically binary devices and have the function described at the end of Sec. 6.4.1.

Although sensing arrays can be formed by using multiple individual sensors, one of the most promising approaches to this problem consists of utilizing an array of electrodes in electrical contact with a compliant conductive material (e.g., graphite-based substances) whose resistance varies as a function of compression. In these devices, often called *artificial skins*, an object pressing against the surface causes local deformations which are measured as continuous resistance variations. The latter are easily transformed into electrical signals whose amplitude is proportional to the force being applied at any given point on the surface of the material.

Several basic approaches used in the construction of artificial skins are shown in Fig. 6.20. The scheme shown in Fig. 6.20*a* is based on a "window" concept, characterized by a conductive material sandwiched between a common ground and an array of electrodes etched on a fiberglass printed-circuit board. Each electrode consists of a rectangular area (and hence the name *window*) which defines one touch point. Current flows from the common ground to the individual electrodes as a function of compression of the conductive material.

In the method shown in Fig. 6.20*b* long, narrow electrode pairs are placed in the same substrate plane with active electronic circuits using LSI technology. The conductive material is placed above this plane and insulated from the substrate plane, except at the electrodes. Resistance changes resulting from material compression are measured and interpreted by the active circuits located between the electrode pairs.

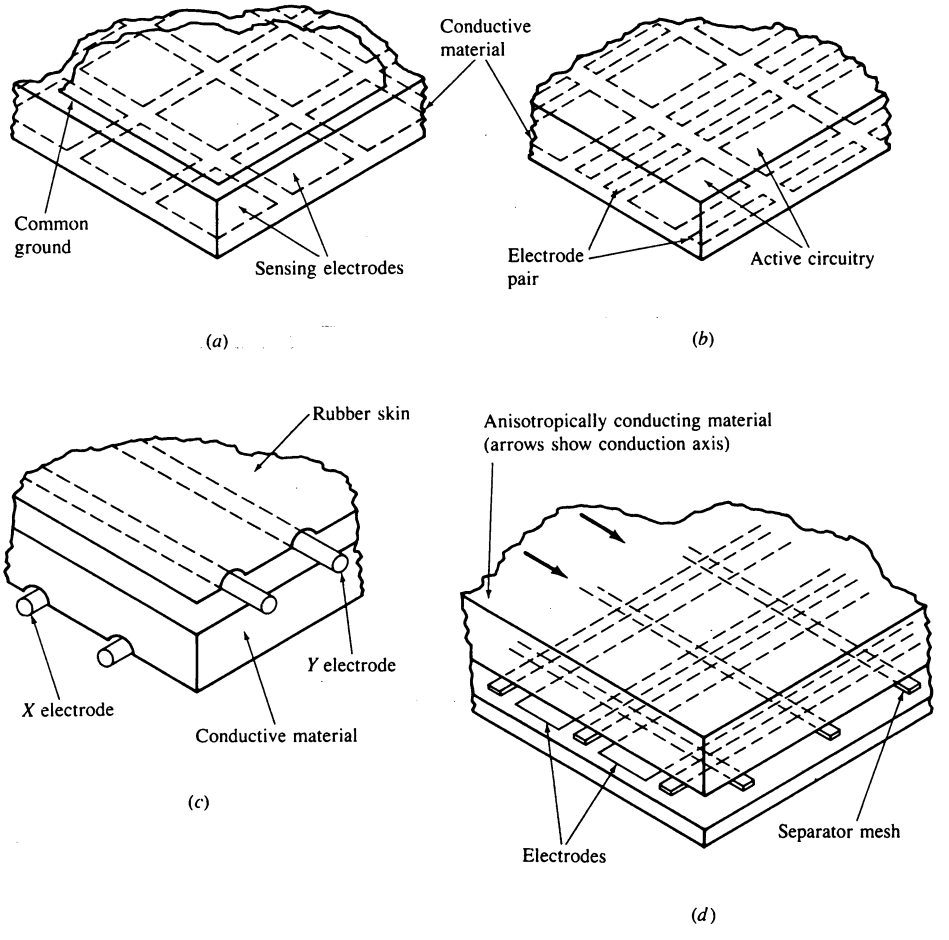

Figure 6.20 Four approaches for constructing artificial skins (see text).

Another possible technique is shown in Fig. 6.20*c*. In this approach the conductive material is located between two arrays of thin, flat, flexible electrodes that intersect perpendicularly. Each intersection, and the conductive material in between, constitutes one sensing point. Changes in resistance as a function of material compression are measured by electrically driving the electrodes of one array (one at a time) and measuring the current flowing in the elements of the other array. The magnitude of the current in each of these elements is proportional to the compression of the material between that element and the element being driven externally.

Finally, the arrangement shown in Fig. 6.20*d* requires the use of an anisotropically conductive material. Such materials have the property of being electrically conductive in only one direction. The sensor is constructed by using a linear array of thin, flat electrodes in the base. The conductive material is placed on top of

this, with the conduction axis perpendicular to the electrodes and separated from them by a mesh so that there is no contact between the material and electrodes in the absence of a force. Application of sufficient force results in contact between the material and electrodes. As the force increases so does the contact area, resulting in lower resistance. As with the method in Fig. 6.20*c*, one array is externally driven and the resulting current is measured in the other. It is noted that touch sensitivity depends on the thickness of the separator.

The methods in Fig. 6.20*c* and *d* are based on sequentially driving the elements of one of the arrays. This often leads to difficulties in interpreting signals resulting from complex touch patterns because of "cross-point" inductions caused by alternate electrical paths. One solution is to place a diode element at each intersection to eliminate current flow through the alternate paths. Another method is to ground all paths, except the one being driven. By scanning the receiving array one path at a time, we are basically able to "look" at the contribution of the individual element intersections.

All the touch sensors discussed thus far deal with measurements of forces normal to the sensor surface. The measurement of tangential motion to determine slip is another important aspect of touch sensing. Before leaving this section, we illustrate this mode of sensing by describing briefly a method proposed by Bejczy [1980] for sensing both the direction and magnitude of slip. The device, illustrated in Fig. 6.21, consists of a free-moving dimpled ball which deflects a thin rod mounted on the axis of a conductive disk. A number of electrical contacts are

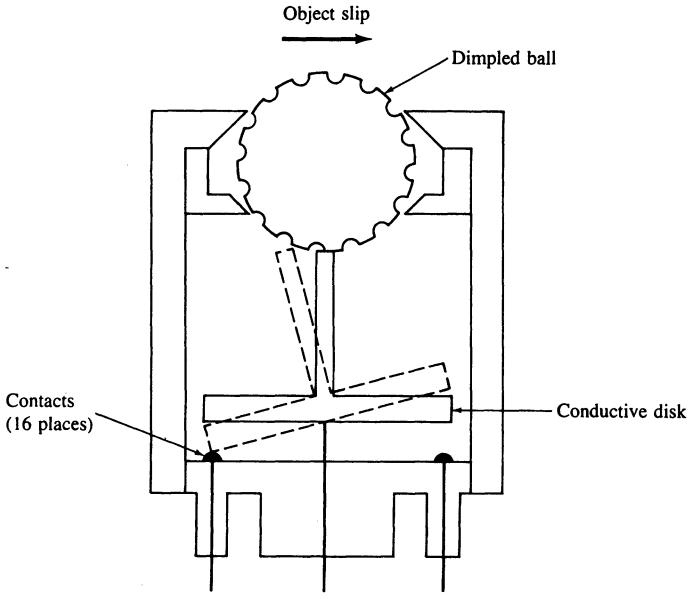

Figure 6.21 A device for sensing the magnitude and direction of slip. (Adapted from Bejczy [1980], © AAAS.)

evenly spaced under the disk. Ball rotation resulting from an object slipping past the ball causes the rod and disk to vibrate at a frequency which is proportional to the speed of the ball. The direction of ball rotation determines which of the contacts touch the disk as it vibrates, pulsing the corresponding electrical circuits and thus providing signals that can be analyzed to determine the average direction of the slip.

6.5 FORCE AND TORQUE SENSING

Force and torque sensors are used primarily for measuring the reaction forces developed at the interface between mechanical assemblies. The principal approaches for doing this are *joint* and *wrist* sensing.† A joint sensor measures the cartesian components of force and torque acting on a robot joint and adds them vectorially. For a joint driven by a dc motor, sensing is done simply by measuring the armature current. Wrist sensors, the principal topic of discussion in this section, are mounted between the tip of a robot arm and the end-effector. They consist of strain gauges that measure the deflection of the mechanical structure due to external forces. The characteristics and analysis methodology for this type of sensor are summarized in the following discussion.

6.5.1 Elements of a Wrist Sensor

Wrist sensors are small, sensitive, light in weight (about 12 oz) and relatively compact in design—on the order of 10 cm in total diameter and 3 cm in thickness, with a dynamic range of up to 200 lb. In order to reduce hysteresis and increase the accuracy in measurement, the hardware is generally constructed from one solid piece of metal, typically aluminum. As an example, the sensor shown in Fig. 6.22 uses eight pairs of semiconductor strain gauges mounted on four deflection bars—one gauge on each side of a deflection bar. The gauges on the opposite open ends of the deflection bars are wired differentially to a potentiometer circuit whose output voltage is proportional to the force component normal to the plane of the strain gauge. The differential connection of the strain gauges provides automatic compensation for variations in temperature. However, this is only a crude first-order compensation. Since the eight pairs of strain gauges are oriented normal to the **x**, **y**, and **z** axes of the force coordinate frame, the three components of force **F** and three components of moment **M** can be determined by properly adding and subtracting the output voltages, respectively. This can be done by premultiplying the sensor reading by a sensor calibration matrix, as discussed in Sec. 6.5.2.

† Another category is *pedestal* sensing, in which strain gauge transducers are installed between the base of a robot and its mounting surface in order to measure the components of force and torque acting on the base. In most applications, however, the base is firmly mounted on a solid surface and no provisions are made for pedestal sensing. The analysis of pedestal sensing is quite similar to that used for wrist sensing, which is discussed in detail in this section.

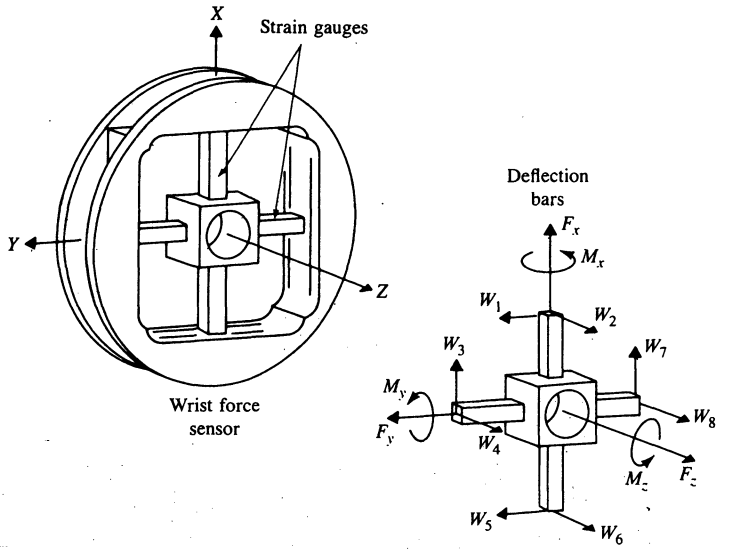

Figure 6.22 Wrist force sensor.

Most wrist force sensors function as transducers for transforming forces and moments exerted at the hand into measurable deflections or displacements at the wrist. It is important that the wrist motions generated by the force sensor do not affect the positioning accuracy of the manipulator. Thus, the required performance specifications can be summarized as follows:

1. *High stiffness.* The natural frequency of a mechanical device is related to its stiffness; thus, high stiffness ensures that disturbing forces will be quickly damped out to permit accurate readings during short time intervals. Furthermore, it reduces the magnitude of the deflections of an applied force/moment, which may add to the positioning error of the hand.
2. *Compact design.* This ensures that the device will not restrict the movement of the manipulator in a crowded workspace. It also minimizes collisions between the sensor and the other objects present in the workspace. With the compact force sensor, it is important to place the sensor as close to the tool as possible to reduce positioning error as a result of the hand rotating through small angles. In addition, it is desirable to measure as large a hand force/moment as possible; thus, minimizing the distance between the hand and the sensor reduces the lever arm for forces applied at the hand.
3. *Linearity.* Good linearity between the response of force sensing elements and the applied forces/moments permits resolving the forces and moments by simple matrix operations. Furthermore, the calibration of the force sensor is simplified. This is discussed in Sec. 6.5.2.

4. *Low hysteresis and internal friction.* Internal friction reduces the sensitivity of the force sensing elements because forces have to overcome this friction before a measurable deflection can be produced. It also produces hysteresis effects that do not restore the position measuring devices back to their original readings.

The wrist force sensor shown in Fig. 6.22 was designed with these criteria taken into consideration.

6.5.2 Resolving Forces and Moments

Assume that the coupling effects between the gauges are negligible, that the wrist force sensor is operating within the elastic range of its material, and that the strain gauges produce readings which vary linearly with respect to changes in their elongation. Then the sensor shown in Fig. 6.22 produces eight raw readings which can be resolved by computer software, using a simple force-torque balance technique, into three orthogonal force and torque components with reference to the force sensor coordinate frame. Such a transformation can be realized by specifying a 6×8 matrix, called the resolved force matrix $\mathbf{R}_F$ (or sensor calibration matrix), which is postmultiplied by the force measurements to produce the required three orthogonal force and three torque components. With reference to Fig. 6.22, the resolved force vector directed along the force sensor coordinates can be obtained mathematically as

$$\mathbf{F} = \mathbf{R}_F\mathbf{W} \tag{6.5-1}$$

where

$$\mathbf{F} \equiv (\text{forces, moments})^T = (F_x, F_y, F_z, M_x, M_y, M_z)^T$$

$$\mathbf{W} \equiv \text{raw readings} = (w_1, w_2, w_3, \ldots, w_8)^T$$

and

$$\mathbf{R}_F = \begin{bmatrix} r_{11} & \cdots & r_{18} \\ \cdot & \cdots & \cdot \\ r_{61} & \cdots & r_{68} \end{bmatrix} \tag{6.5-2}$$

In Eq. (6.5-2), the $r_{ij} \neq 0$ are the factors required for conversion from the raw reading $\mathbf{W}$ (in volts) to force/moment (in newton-meters). If the coupling effects between the gauges are negligible, then by looking at Fig. 6.22 and summing the forces and moments about the origin of the sensor coordinate frame located at the center of the force sensor, we can obtain the above equation with some of the r_{ij}

equal to zero. With reference to Fig. 6.22, the resolved force matrix in Eq. (6.5-2) becomes

$$\mathbf{R}_F = \begin{bmatrix} 0 & 0 & r_{13} & 0 & 0 & 0 & r_{17} & 0 \\ r_{21} & 0 & 0 & 0 & r_{25} & 0 & 0 & 0 \\ 0 & r_{32} & 0 & r_{34} & 0 & r_{36} & 0 & r_{38} \\ 0 & 0 & 0 & r_{44} & 0 & 0 & 0 & r_{48} \\ 0 & r_{52} & 0 & 0 & 0 & r_{56} & 0 & 0 \\ r_{61} & 0 & r_{63} & 0 & r_{65} & 0 & r_{67} & 0 \end{bmatrix} \tag{6.5-3}$$

Quite often, this assumption is not valid and some coupling does exist. For some force sensors, this may produce as much as 5 percent error in the calculation of force resolution. Thus, in practice, it is usually necessary to replace the resolved force matrix $\mathbf{R}_F$ by a matrix which contains 48 nonzero elements. This "full" matrix is used to calibrate the force sensor, as discussed in Sec. 6.5.3. The resolved force vector $\mathbf{F}$ is used to generate the necessary error actuating control signal for the manipulator. The disadvantage of using a wrist force sensor is that it only provides force vectors resolved at the assembly interface for a single contact.

6.5.3 Sensor Calibration

The objective of calibrating the wrist force sensor is to determine all the 48 unknown elements in the resolved force matrix [Eq. (6.5-2)], based on experimental data. Due to the coupling effects, we need to find the full 48 nonzero elements in the $\mathbf{R}_F$ matrix. The calibration of the wrist force sensor is done by finding a pseudoinverse calibration matrix $\mathbf{R}_F^*$ which satisfies

$$\mathbf{W} = \mathbf{R}_F^* \mathbf{F} \tag{6.5-4}$$

and

$$\mathbf{R}_F^* \mathbf{R}_F \cong \mathbf{I}_{8\times 8} \tag{6.5-5}$$

where $\mathbf{R}_F^*$ is an 8×6 matrix and $\mathbf{I}_{8\times 8}$ is an 8×8 identity matrix. Then the calibration matrix $\mathbf{R}_F$ from Eq. (6.5-1) can be found from the pseudoinverse of $\mathbf{R}_F^*$ in Eq. (6.5-4) using a least-squares-fit technique. Premultiplying Eq. (6.5-4) by $(\mathbf{R}_F^*)^T$, we have

$$(\mathbf{R}_F^*)^T \mathbf{W} = [(\mathbf{R}_F^*)^T \mathbf{R}_F^*]\mathbf{F} \tag{6.5-6}$$

Inverting the matrix $[(\mathbf{R}_F^*)^T \mathbf{R}_F^*]$ yields

$$\mathbf{F} = [(\mathbf{R}_F^*)^T \mathbf{R}_F^*]^{-1} (\mathbf{R}_F^*)^T \mathbf{W} \tag{6.5-7}$$

Therefore comparing Eq. (6.5-1) and Eq. (6.5-7), we have

$$\mathbf{R}_F \cong [(\mathbf{R}_F^*)^T\mathbf{R}_F^*]^{-1}(\mathbf{R}_F^*)^T \tag{6.5-8}$$

The $\mathbf{R}_F^*$ matrix can be identified by placing known weights along the axes of the sensor coordinate frame. Details about the experimental procedure for calibrating the resolved force matrix can be found in a paper by Shimano and Roth [1979].

6.6 CONCLUDING REMARKS

The material presented in this chapter is representative of the state of the art in external robot sensors. It must be kept in mind, however, that the performance of these sensors is still rather primitive when compared with human capabilities.

As indicated at the beginning of this chapter, the majority of present industrial robots perform their tasks using preprogrammed techniques and without the aid of sensory feedback. The relatively recent widespread interest in flexible automation, however, has led to increased efforts in the area of sensor-driven robotic systems as a means of increasing the scope of application of these machines. Thus, sensor development is indeed a dynamic field where new techniques and applications are commonplace in the literature. For this reason, the topics included in this chapter were selected primarily for their value as fundamental material which would serve as a foundation for further study of this and related fields.

REFERENCES

Several survey articles on robotic sensing are Rosen and Nitzan [1977], Bejczy [1980], Galey and Hsia [1980], McDermott [1980], and Merritt [1982]. Further reading on laser range finders may be found in Duda et al. [1979] and Jarvis [1983*a*, 1983*b*]. For further reading on the material in Sec. 6.3 see Spencer [1980], Catros and Espiau [1980], and Canali et al. [1981*a*, 1981*b*]. Further reading for the material in Sec. 6.4 may be found in Harmon [1982], Hillis [1982], Marck [1981], and Raibert and Tanner [1982]. See also the papers by Beni et al. [1983], McDermott [1980], and Hackwood et al. [1983]. Pedestal sensors (Sec. 6.5) are discussed by Drake [1977]. Additional reading on force-torque sensing may be found in Nevins and Whitney [1978], Shimano and Roth [1979], Meindl and Wise [1979], and Wise [1982].

PROBLEMS

6.1 Show the validity of Eq. (6.2-8).

6.2 A sheet-of-light range sensor illuminating a work space with two objects produced the following output on a television screen:

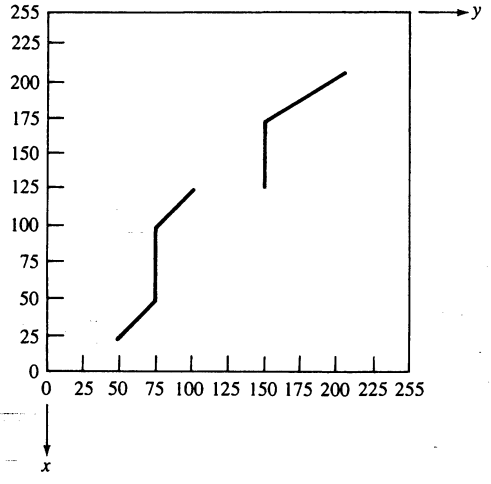

Assuming that the ranging system is set up as in Fig. 6.3*b* with $M = 256$, $D_0 = 1$ m, $D_c = 2$ m, $B = 3$ m, and $\lambda = 35$ mm, obtain the distance between the objects in the direction of the light sheet.

6.3 (*a*) A helium-neon (wavelength 632.8 nm) continuous-beam laser range finder is modulated with a 30-MHz sine wave. What is the distance to an object that produces a phase shift of 180°? (*b*) What is the upper limit on the distance for which this device would produce a unique reading?

6.4 Compute the upper limit on the frequency of a modulating sine wave to achieve a working distance of up to (but not including) 5 m using a continuous-beam laser range finder.

6.5 (*a*) Suppose that the accuracy of a laser range finder is corrupted by noise with a gaussian distribution of mean 0 and standard deviation of 100 cm. How many measurements would have to be averaged to obtain an accuracy of ± 0.5 cm with a .95 probability? (*b*) If, instead of being 0, the mean of the noise were 5 cm, how would you compensate the range measurements for this effect?

6.6 With reference to Fig. 6.15, give a set of waveforms for an ultrasonic sensor capable of measuring range instead of just yielding a binary output associated with proximity.

6.7 Suppose that an ultrasonic proximity sensor is used to detect the presence of objects within 0.5 m of the device. At time $t = 0$ the transducer is pulsed for 0.1 ms. Assume that it takes 0.4 ms for resonances to die out within the transducer and 20 ms for echoes in the environment to die out. Given that sound travels at 344 m/s: (*a*) What range of time should be used as a window? (*b*) At what time can the device be pulsed again? (*c*) What is the minimum detectable distance?

6.8 An optical proximity sensor (Fig. 6.16) has a sensitive volume formed by the intersection of two identical beams. The cone formed by each beam originates at the lens and has a vertex located 4 cm in front of the center of the opposite lens. Given that each lens has a diameter of 4 mm, and that the lens centers are 6 mm apart, over what approximate range will this sensor detect an object? Assume that an object is detected anywhere in the sensitive volume.

6.9 A 3×3 touch array is scanned by driving the rows (one at a time) with 5 V. A column is read by holding it at ground and measuring the current. Assume that the

undriven rows and unread columns are left in high impedance. A given force pattern against the array results in the following resistances at each electrode intersection (row, column): 100 Ω at (1, 1), (1, 3), (3, 1), and (3, 3); and 50 Ω at (2, 2) and (3, 2). All other intersections have infinite resistance. Compute the current measured at each row-column intersection in the array, taking into account the cross-point problem.

6.10 Repeat Prob. 6.9 assuming (*a*) that all undriven rows and all columns are held at ground; and (*b*) that a diode (0.6 voltage drop) is in series with the resistance at each junction.

6.11 A wrist force sensor is mounted on a PUMA robot equipped with a parallel jaw gripper and a sensor calibration procedure has been performed to obtain the calibration matrix $\mathbf{R}_F$. Unfortunately, after you have performed all the measurements, someone remounts a different gripper on the robot. Do you need to recalibrate the wrist force sensor? Justify your answer.